iScience

CellPress
OPEN ACCESS

Article

Cross-species comparative hippocampal transcriptomics in Alzheimer's disease

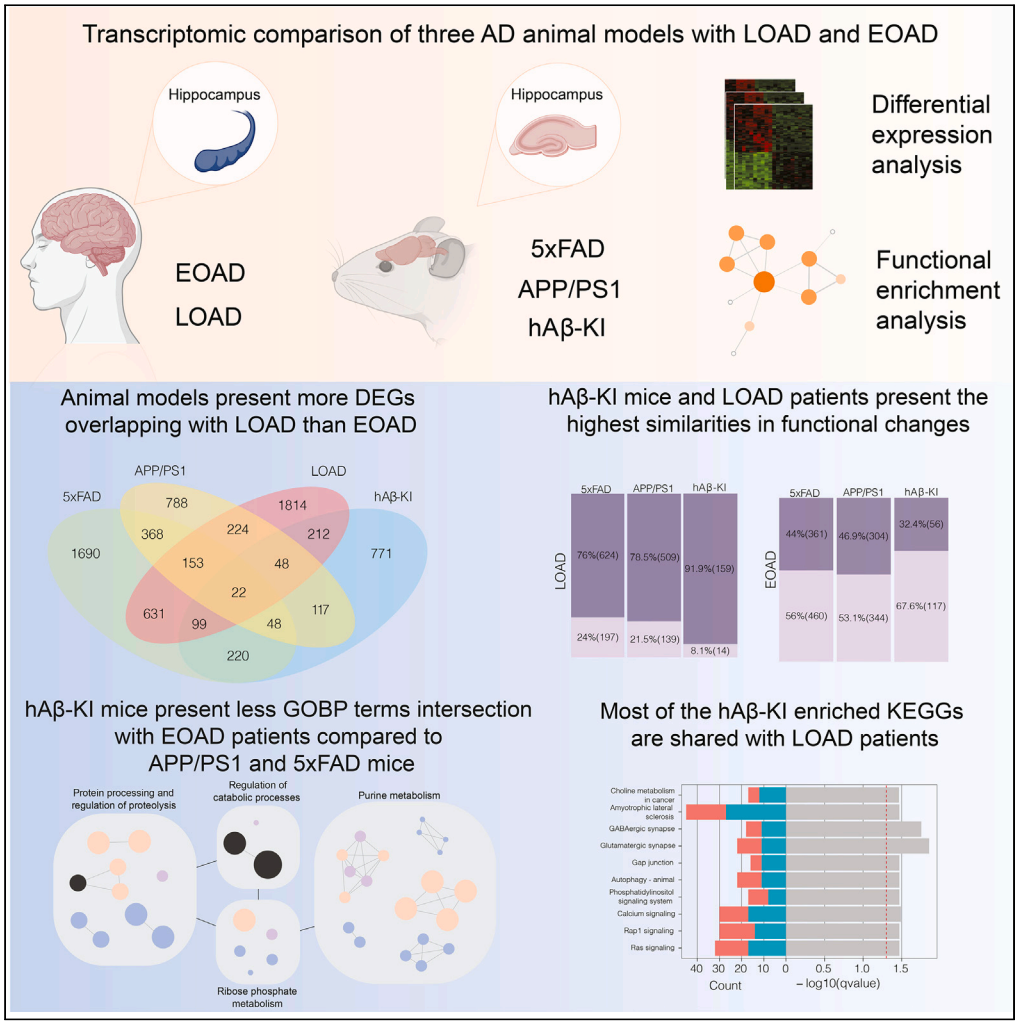

Marco Antônio De Bastiani, Bruna Bellaver, Giovanna Carello-Collar, ..., Mychael V. Lourenco, Pedro Rosa-Neto, Eduardo R. Zimmer

eduardo.zimmer@ufrgs.br

Highlights

More biological processes than genes change in human pathology than in mouse models of AD

Mouse models of AD had more transcriptomic similarities to LOAD than to EOAD

HAβ-KI model had the most proportion overlap of biological process alterations to LOAD

De Bastiani et al., iScience *27*, 108671
January 19, 2024
https://doi.org/10.1016/j.isci.2023.108671

iScience

CellPress
OPEN ACCESS

Article

Cross-species comparative hippocampal transcriptomics in Alzheimer's disease

Marco Antônio De Bastiani,[1,13] Bruna Bellaver,[8,13] Giovanna Carello-Collar,[1] Maria Zimmermann,[2,3] Peter Kunach,[2,3,4] Ricardo A.S. Lima-Filho,[5] Stefania Forner,[6] Alessandra Cadete Martini,[7] Tharick A. Pascoal,[8,9] Mychael V. Lourenco,[5] Pedro Rosa-Neto,[2,3,4] and Eduardo R. Zimmer[1,10,11,12,14,*]

SUMMARY

Alzheimer's disease (AD) is a multifactorial pathology, with most cases having a sporadic origin. Recently, knock-in (KI) mouse models, such as the novel humanized amyloid-β (hAβ)-KI, have been developed to better resemble sporadic human AD. METHODS: Here, we compared hippocampal publicly available transcriptomic profiles of transgenic (5xFAD and APP/PS1) and KI (hAβ-KI) mouse models with early- (EOAD) and late- (LOAD) onset AD patients. RESULTS: The three mouse models presented more Gene Ontology biological processes terms and enriched signaling pathways in common with LOAD than with EOAD individuals. Experimental validation of consistently dysregulated genes revealed five altered in mice (SLC11A1, S100A6, CD14, CD33, and C1QB) and three in humans (S100A6, SLC11A1, and KCNK). Finally, we identified 17 transcription factors potentially acting as master regulators of AD. CONCLUSION: Our cross-species analyses revealed that the three mouse models presented a remarkable similarity to LOAD, with the hAβ-KI being the more specific one.

INTRODUCTION

Alzheimer's disease (AD) is commonly categorized into early- (EOAD; <65 years-old) and late- (LOAD; ≥65 years-old) onset based on the age of clinical onset, the latter being the most prevalent form of the disease.[1] This broad definition includes the mendelian and non-mendelian EOAD, which confers an additional degree of heterogeneity to this group. Both forms of EOAD seem to present more prominent brain atrophy, glucose hypometabolism, and increased tau positron emission tomography (PET) uptake compared to LOAD.[2–6] However, a recent study demonstrated a similar biomarker profile between autosomal dominant EOAD and LOAD patients, supporting a shared pathobiological construct between both forms of the disease.[7]

Autosomal dominant inheritance mendelian EOAD accounts for less than 1% of AD cases, but gene mutations found in these patients have been used for developing most AD models.[1] Specifically, mouse models overexpressing one or more mutations in the amyloid precursor protein (APP), presenilin 1 (PSEN1), and presenilin 2 (PSEN2) genes have dominated the AD experimental research. However, these models have undergone extensive scrutiny in the past years because they present artifacts introduced by APP overexpression and do not resemble important aspects of LOAD.[8–10] Thus, a major challenge in the field has been the development of animal models that better recapitulate LOAD. The emergence of a new knock-in (KI) strategy for developing novel models expressing human APP with appropriate levels and cellular specificity seems to provide improved models for investigating sporadic AD.[10–12]

The investigation of core molecular programs shared by overexpression and KI models with human pathology may help determine to what extent animal models can resemble human disease. Additionally, the ability to recapitulate key molecular pathways activated or repressed in AD is crucial for model validity. Here, we aimed to ascertain the genes and pathways overlapping gene overexpression (5xFAD and APP/PS1)

[1]Graduate Program in Biological Sciences: Biochemistry, Department of Biochemistry, Institute of Health Basic Sciences, Universidade Federal do Rio Grande do Sul (UFRGS), Porto Alegre, State of Rio Grande do Sul 90035-003, Brazil
[2]Department of Neurology and Neurosurgery, Montréal Neurological Institute, McGill University, Montréal, Québec H3A 1A1, Canada
[3]Translational Neuroimaging Laboratory, McGill University, Montréal, Québec H4H 1R3, Canada
[4]Douglas Hospital Research Centre, Montreal, Québec H4H 1R3, Canada
[5]Institute of Medical Biochemistry Leopoldo de Meis, Federal University of Rio de Janeiro, Rio de Janeiro, State of Rio de Janeiro 21941-902, Brazil
[6]Institute for Memory Impairments and Neurological Disorders (UCI MIND), University of California, Irvine, Irvine, CA 92697, USA
[7]Department of Pathology & Laboratory Medicine, University of California, Irvine, Irvine, CA 92697, USA
[8]Department of Psychiatry, School of Medicine, University of Pittsburgh School of Medicine, Pittsburgh, PA 15213, USA
[9]Department of Neurology, School of Medicine, University of Pittsburgh School of Medicine, Pittsburgh, PA 15213, USA
[10]Department of Pharmacology, ICBS, UFRGS, Porto Alegre, State of Rio Grande do Sul 90035-003, Brazil
[11]Graduate Program in Biological Sciences: Pharmacology and Therapeutics, Department of Pharmacology, ICBS, UFRGS, Porto Alegre, State of Rio Grande do Sul 90035-003, Brazil
[12]Brain Institute of Rio Grande Do Sul, Pontifical Catholic University of Rio Grande Do Sul, Porto Alegre, State of Rio Grande do Sul 90610-000, Brazil
[13]These authors contributed equally
[14]Lead contact
*Correspondence: eduardo.zimmer@ufrgs.br
https://doi.org/10.1016/j.isci.2023.108671

and KI [humanized amyloid-β(Aβ)-KI] mouse models with EOAD and LOAD. With this in mind, we compared the hippocampal transcriptomic profiles of these animal models and AD and established the molecular similarity and specificity of mouse data to the human disease. We further employed a regulatory network-based approach to infer and investigate common master regulators between animal models and AD. Finally, we validated our transcriptomic exploratory findings in the hippocampus of APP/PS1 mice and *postmortem* EOAD and LOAD individuals.

RESULTS

hAβ-KI, 5xFAD, and APP/PS1 models exhibit more differentially expressed genes overlapping with LOAD than EOAD

We first investigated the genes that are differentially expressed between non-AD [wild type (WT, for animal models) and cognitively unimpaired individuals (CU, for EOAD and LOAD)] and AD conditions. Differential expression analysis of the hippocampus of hAβ-KI, 5xFAD, and APP/PS1 mice and WT controls identified 1537, 3231, and 1768 differentially expressed genes (DEGs), respectively (unadjusted p value <0.05; Figures 1B, 1C, and S1; Table S1). Next, to investigate the discrepancies in gene expression between the three AD animal models and human AD subtypes, we evaluated the overlap between DEGs. We found that the hAβ-KI animals presented more DEGs overlapping with the 5xFAD mice than with APP/PS1 model [389 (25.3%) versus 235 (15.3%) DEGs, respectively; Chi-square adjusted p value <0.001; Figure 1D]. In addition, the comparison with AD human data demonstrated that hAβ-KI mice exhibited more DEGs in common with LOAD than with EOAD individuals [381 (24.8%) versus 164 (10.7%), respectively; Figures 1E and 1F]. Despite being mouse models carrying familial AD-linked mutations, APP/PS1 and 5xFAD mice shared more DEGs with LOAD than with EOAD patients (Figures 1E and 1F). Moreover, considering the total of DEGs identified in the mouse models as reference (model-disease overlap), the intersection of DEGs between 5xFAD and EOAD was significantly higher (14%) than the overlap between both APP/PS1 (10.9%; Chi-square adjusted p value = 0.0061) or hAβ-KI (10.7%; Chi-square adjusted p value = 0.0054) with EOAD (Figure 1E - right). On the other hand, the overlap of LOAD DEGs with 5xFAD (28%) and with APP/PS1 (25.3%) mice was not significantly different from the overlap with hAβ-KI (24.8%; Figure 1F - right; Chi-square adjusted p value = 0.123 and Chi-square adjusted p value = 0.063, respectively). Interestingly, the hAβ-KI model shared 212 DEGs exclusively with LOAD, while only 98 with EOAD (Figures 1B and 1C). Comparing only the adjusted p value DEGs [Benjamini & Hochberg (BH) < 0.1], we observed a similar profile of gene overlap, especially regarding the hAβ-KI model and LOAD (Figure S2). However, no overlap of DEGs was identified between all animal models and LOAD or EOAD when considering adjusted p value DEGs <0.05 (Figure S3; Table S2). Thus, we opted for using unadjusted p values <0.05 for subsequent functional enrichment analysis, which allows for exploratory cross-species investigation of core molecular programs that can be further validated. Only seven DEGs were found in common with all the mouse models and human AD. Among them, DEGs related to innate immune response (C1QB, CD33, CD14, S100A6, and SLC11A1) were consistently upregulated across the groups, while those related to membrane potential regulation and neuropeptide production (KCNK1 and SST) were mostly downregulated. Additional material related to STAR Methods can be found in Tables S6, S7, S8, and S9.

Because functional activity of proteins is highly dependent on their interactions with other proteins, understanding protein interactions is crucial to uncover their role. The protein-protein interaction (PPI) network of DEGs intersecting the hAβ-KI model and LOAD patients revealed that PTGES3, GNB1, ARIH2, SMURF1, and EIF3A genes are hubs of the four clusters formed (Figure 1G). However, only two genes revealed in the PPI network – GNB1 and NKTR – were differentially expressed in the hAβ-KI model after BH adjustment. Considering the DEGs exclusively shared with the hAβ-KI model and EOAD patients, only 11 remained in the PPI network, and only the PRPF40A gene remained significant in hAβ-KI after multiple comparisons correction (Figure 1H). Next, we compared the DEGs of each mouse model with a database from multiple sclerosis (MS) patients to verify their specificity for AD pathology. The three mouse models presented a greater overlap of DEGs with AD than with MS individuals (Figures 1I, 1J, S4A, and S4B). Interestingly, no significant differences were observed in DEGs shared between hAβ-KI mice and EOAD (10.7%) or MS patients (9.6%; Figures 1K and S4C), while the overlap of hAβ-KI DEGs with LOAD was significantly higher than with both EOAD and MS (24.8%; Chi-square adjusted p value <0.001; Figures 1K and S4C).

To validate our exploratory transcriptomic findings, we performed qRT-PCR analyses of the seven DEGs overlapping between human AD and animal models (Tables S10 and 11). The validation was performed in APP/PS1, LOAD, and EOAD *postmortem* hippocampus. Significant increases in S100A6, C1QB, CD33, CD14, and SLC11A1 mRNA levels were observed in APP/PS1 mice compared to WT littermates (Figure 2A). Regarding the human hippocampal tissue validation, S100A6 was significantly increased in LOAD and EOAD compared to CU individuals (Figure 2B). In addition, SLC11A1 expression increased, while KCNK significantly decreased in LOAD individuals. Although C1QB, CD33, and CD14 presented decrease/increase trends in AD patients compared to CU individuals, they did not reach statistical significance.

DEGs found in neurons and oligodendrocytes are the majority among all animal models and AD subtypes

We next explored which brain cell types were more associated with the DEGs observed in each animal model and the AD subtypes. In the 5xFAD and APP/PS1 models, neuron was the cell type with more DEGs between the transgenic animals and their WT controls (1368 and 636, respectively, Table 1). Oligodendrocytes and neurons were the cell types with the most DEGs for hAβ-KI (632 and 540, respectively) and for EOAD (658 and 558, respectively, Table 1). Finally, endothelial cells were associated with most of the DEGs observed in LOAD (620, Table 1) cases compared to CU individuals. Interestingly, despite these animal models and AD subtypes share a fair amount of DEGs, the majority of DEGs, derived especially from neurons and oligodendrocytes, are unique for each group (Figure S4).

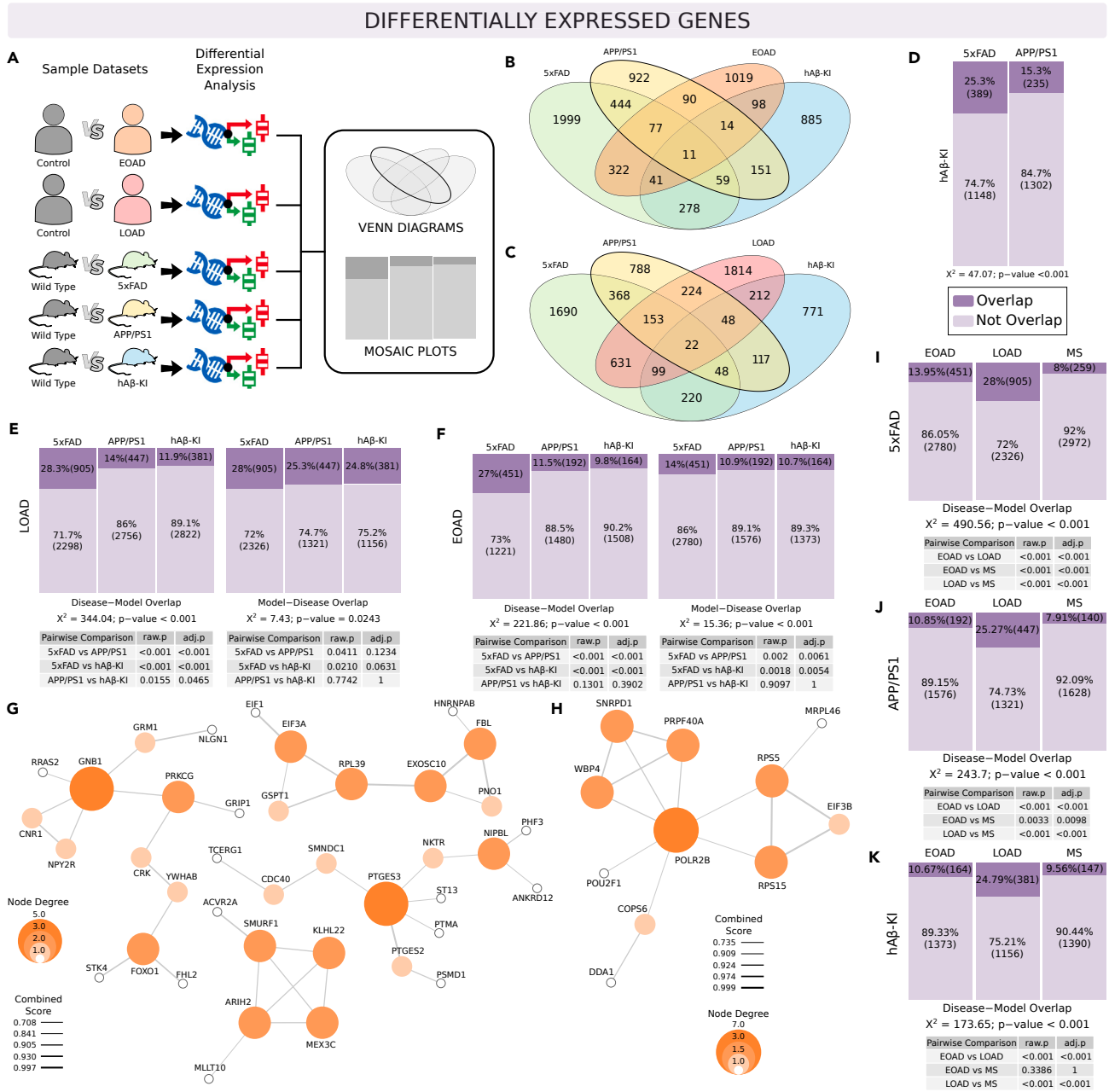

Figure 1. Shared DEGs among EOAD, LOAD, and mouse models of AD

Schematic summary of samples used and analysis workflow to obtain DEGs. (A) Venn diagram showing DEGs overlap between EOAD (B) and LOAD (C) with 5xFAD, APP/PS1, and hAβ-KI mice. Mosaic plot of hAβ-KI, 5xFAD, and APP/PS1 overlap (D) Mosaic plot of EOAD-model (left) and model-EOAD (right) DEGs overlap with 5xFAD, APP/PS1, and hAβ-KI mice (E) Mosaic plot of LOAD-model (left) and model-LOAD (right) DEGs overlap with 5xFAD, APP/PS1, and hAβ-KI mice (F) PPI network of DEGs exclusively shared between hAβ-KI mice and LOAD (G) or EOAD (H) patients. Mosaic plot of EOAD, LOAD, or MS DEGs overlaps with 5xFAD mice (I) Mosaic plot of EOAD, LOAD, or MS DEGs overlaps with APP/PS1 mice (J) Mosaic plot of EOAD, LOAD, or MS DEGs overlaps with hAβ-KI mice (K) The size of red and yellow boxes reflects the proportion of overlapping and non-overlapping DEGs, respectively. Pearson's Chi−squared test with Yates' continuity correction was applied for the mosaic plot analysis. EOAD, early-onset Alzheimer's disease; LOAD, late-onset Alzheimer's disease; MS, multiple sclerosis; hAβ-KI, humanized amyloid-β knock-in. Genes with unadjusted p value <0.05 were considered as DEGs.

hAβ-KI mice and LOAD patients present higher similarities in functional changes

We next investigated the larger biological processes in which the DEGs found for each animal model/AD subtype are involved. Functional enrichment analysis of Gene Ontology for biological processes (GOBPs) revealed that ~92% of the GOBPs enriched in hAβ-KI mice overlap

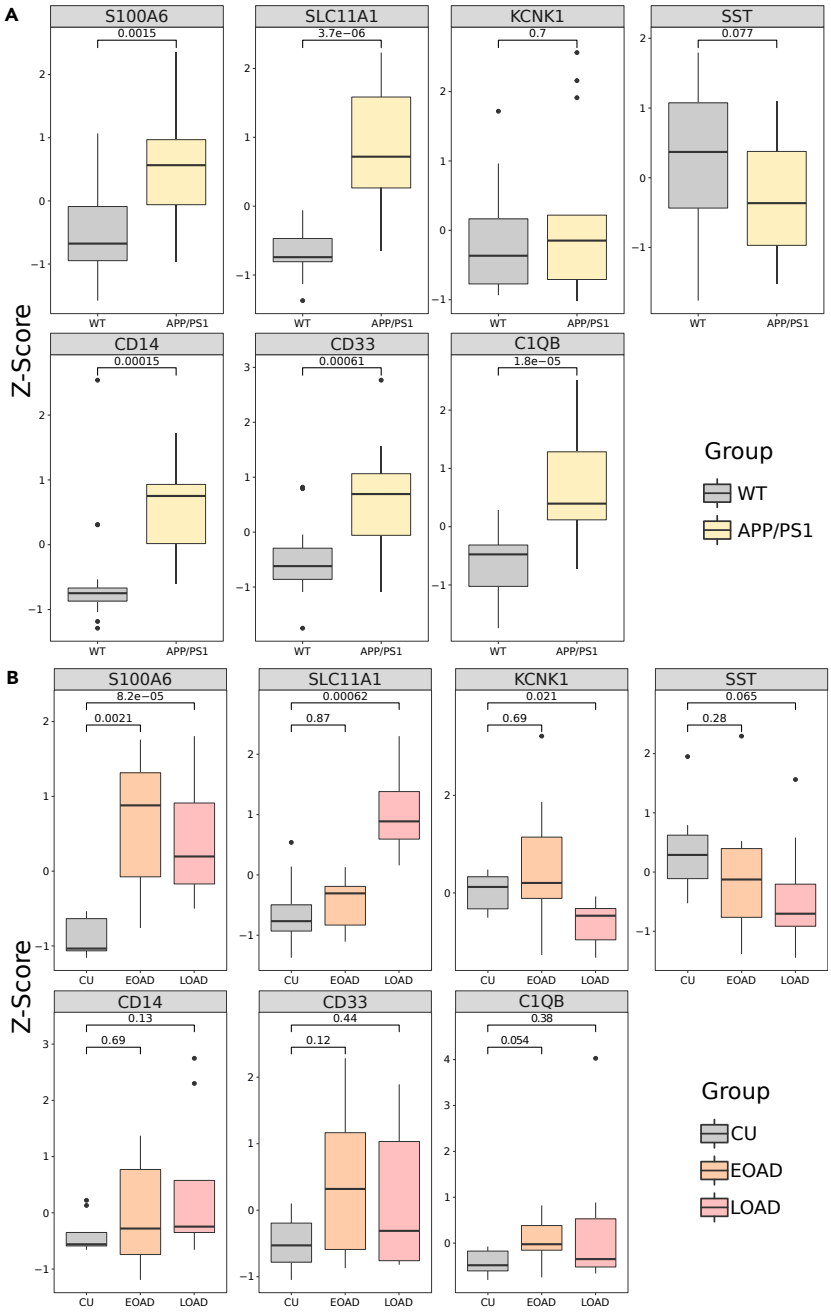

Figure 2. Experimental validation of exploratory transcriptomics findings

The expression of seven genes overlapping between AD and animal models were evaluated by qRT-PCR in the hippocampus from APP/PS1 (n = 14) and WT (n = 14) mice from two independent laboratories (A) and in CU individuals (n = 9), early- (EOAD, n = 7) and late- (LOAD, n = 8) onset AD patients from the Douglas-Bell Canada Brain Bank.

(B) Standard scores (*Z* score) of APP/PS1, EOAD, and LOAD were compared for their difference from control using Wilcoxon.

with enriched terms in LOAD patients in the model-disease approach (Figures 3C and 3F - right), while the intersection with EOAD was markedly low (around 32%, Figures 3C and 3F - right). The remaining 8% of GOBP terms not shared between hAβ-KI mice and LOAD were related to RNA splicing and protein phosphorylation (Table S4). Additionally, the hAβ-KI mice presented a higher number of enriched GOBP terms in joint with 5xFAD (79.2%) than with APP/PS1 (56.1%) model (Figure 3D; Chi-square adjusted p value <0.001). Surprisingly, 5xFAD and APP/PS1 shared more than 75% of their enriched GOBPs with LOAD (Figures 3C and 3F - right) and only ~45% with EOAD (Figures 3B and 3E – right). However, we observed that about 50% of GOBPs overlap between 5xFAD and EOAD or LOAD, indicating a lack of disease subtype specificity

Table 1. Number of differentially expressed genes by each brain cell type

	Differentially expressed genes (n)				
Animal model/AD subtype	Astrocytes	Endothelial cells	Microglia	Neurons	Oligodendrocytes
5xFAD	249	595	157	1368	339
APP/PS1	415	659	918	936	400
hAB-KI	355	459	472	540	632
LOAD	168	620	263	230	226
EOAD	302	223	308	558	658

EOAD, early-onset Alzheimer's disease; LOAD, late-onset Alzheimer's disease; MS, multiple sclerosis; hAβ-KI, humanized amyloid-β knock-in.

for this model. The comparison among the GOBPs of the three models with MS demonstrated, however, greater specificity of these mouse models for AD (Figure S5). Indeed, Figures 2G–2I show that all mouse models evaluated presented less than 5% of enriched GOBP terms in common with MS.

hAβ-KI mice present less GOBP terms intersection with EOAD patients compared to APP/PS1 and 5xFAD mice

As our initial analyses revealed several enriched GOBP terms, we computed the semantic similarity among GO terms to understand better the global processes represented by them. The union of enriched GOBP intersecting terms in the mouse models and human AD was generated to better visualize the common biological processes altered in each group. "Regulation of cytokine secretion" (13 nodes), "regulation of catabolic processes" (3 nodes), "NF-κB signaling" (9 nodes), and "intracellular transport and secretion" (21 nodes) were among the GOBP terms enriched in the hippocampus of the three mouse models and EOAD patients (Figures 4 and S6; light gray circles). These terms are mainly related to cellular response to stressor agents, hormones and cytokines, immune response, and calcium homeostasis and transport. Interestingly, GOBP terms related to oxidative phosphorylation found in EOAD are only enriched in the APP/PS1 model (purple circles).

hAβ-KI mice and LOAD patients exhibit greater overlap among the enriched GOBP terms

Similarly, we computed the semantic similarity among GOBP terms and compared the overlap with GOBP present in LOAD. Figure 5 shows that hAβ-KI mice GOBP terms are more represented among the GOBPs in common with LOAD (circles in shades of gray) than with EOAD (Figure S7). "PI3K and NFkB signaling pathways" (20 nodes), "regulation of neuronal development" (19 nodes), "regulation of neurotransmitter and hormone secretion" (31 nodes), "regulation of immune response" (22 nodes), "antigen processing and presentation" (21 nodes), and "phospholipid and ribose phosphate metabolism" (10 nodes) are among the enriched biological processes shared between all three mouse models and LOAD (pink circles). Interestingly, "glucose, cholesterol, and purine metabolism", "regulation of MAPK cascade", and "calcium homeostasis" only appeared enriched in 5xFAD and APP/PS1 mice (gray circles).

Most of the hAβ-KI enriched KEGGs are shared with LOAD patients

The most affected pathways related to changes in the transcriptome profile were identified using enrichment analysis of Kyoto Encyclopedia of Genes and Genomes (KEGG) canonical pathways. Figures 6A and 6B show that among the 10 KEGGs found significantly enriched in the hAβ-KI model, six were also identified in LOAD patients ["glutamatergic and GABAergic synapse" (adjusted p value = 0.017), "calcium signaling" (adjusted p value = 0.040), "Rap1 and Ras signaling" (adjusted p value = 0.040), and "choline metabolism in cancer" (adjusted p value = 0.041)], while only one was enriched in EOAD patients ["amyotrophic lateral sclerosis" (adjusted p value = 0.040); Table S5]. KEGG analysis also revealed that APP/PS1 was the mouse model that presented the highest percentage of pathway overlap with EOAD (36.7%; Figure 6C) and LOAD (73.3%; Figure 6D). Interestingly, most of the intersection between APP/PS1 and human AD is represented by KEGGs related to other neurodegenerative diseases [e.g., Parkinson's disease, Huntington's disease (HD)] or bacterial infection (e.g., *Escherichia coli*, *Salmonella* spp.; Table S5). Despite PI3K pathway-related GOBPs appearing enriched in LOAD, they were only significantly altered in the hAβ-KI model (adjusted p value = 0.040) in the KEGG analysis. "Rap1 and Ras signaling pathways" and "adhesion and apoptosis" were found consistently altered in the APP/PS1 and hAβ-KI models (Figures 6H and 6I; Table S5). In addition, the 5xFAD was the mouse model that presented more enriched KEGG terms (Figure 6G; Table S5). Similar to the GOBP enrichment analysis, 5xFAD presented more pathways shared with LOAD (56.9%) than with EOAD (13.8%; Figures 6C and 6D), which were mainly related to synaptic neurotransmission and insulin regulation (Table S5). Additionally, alterations in apoptosis- and endocannabinoid system-related pathways were observed in the 5xFAD model and the human disease (Table S5). Despite an overlap in KEGGs associated with inflammatory diseases and bacterial infections between 5xFAD and AD, well-studied signaling pathways in the context of inflammation were only observed in the 5xFAD model (e.g., TNF, Toll-like, NF-κB).

EOAD and LOAD patients share two enriched master regulators with overexpressing and knock-in AD mouse models

To identify elements located in higher positions of the biological system hierarchy, we performed a master regulator (MR) analysis to determine transcription factors potentially driving the biological alterations observed in AD. In addition, we asked if these elements were also

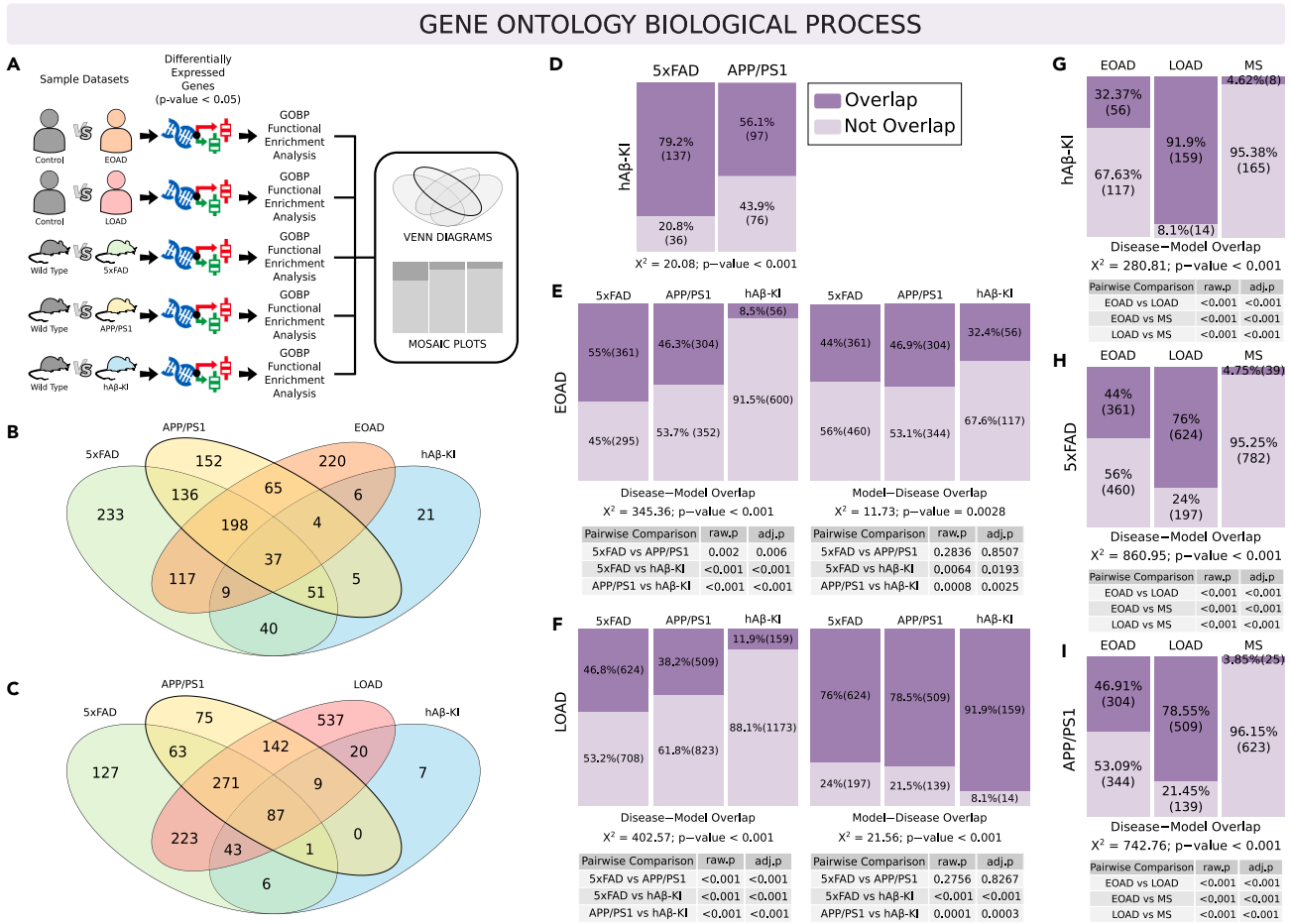

Figure 3. GOBP overlap among EOAD, LOAD, and mouse models of AD

Schematic summary of samples used and analysis workflow to obtain GOBPs. (A) Venn diagram of GOBPs intersections in EOAD (B) and LOAD (C) with 5xFAD, APP/PS1, and hAβ-KI mice. Mosaic plot of hAβ-KI-5xFAD and -APP/PS1 GOBP overlap (D) Mosaic plot of EOAD-model (left) and model-EOAD (right) GOBP overlap with 5xFAD, APP/PS1, and hAβ-KI mice (E) Mosaic plot of LOAD-model (left) and model-LOAD (right) GOBP overlap with 5xFAD, APP/PS1, and hAβ-KI mice (F) Mosaic plot of EOAD, LOAD, or MS GOBP overlap with 5xFAD mice (G) Mosaic plot of EOAD, LOAD, or MS GOBP overlap with APP/PS1 mice. (H) Mosaic plot of EOAD, LOAD, or MS GOBP overlap with hAβ-KI mice. (I) The size of the red and yellow boxes reflects the proportion of overlapping and non-overlapping GOBPs, respectively. Pearson's Chi−squared test with Yates' continuity correction was applied for the mosaic plot analysis. EOAD, early-onset Alzheimer's disease; LOAD, late-onset Alzheimer's disease; MS, multiple sclerosis; hAβ-KI, humanized amyloid-β knock-in.

orchestrating the transcriptional profile changes in mouse models. Our analysis revealed 95 MR enriched within DEGs emerging in at least one experimental group (Figures 7A and 7B; Table S6). Interestingly, both 5xFAD and APP/PS1 mouse models presented more MR in common with LOAD than with EOAD, while hAβ-KI mice exhibited a similar overlap with both subtypes of human AD (Figures 7A and 7B). Among the 17 MR identified in ≥4 groups, only PARK2 and SOX9 were enriched in the three models and in the human disease (Figure 7C). Next, two-tail gene set enrichment analysis (GSEA) was performed to infer the activation state of each candidate. We observed that, while PARK2 is repressed, SOX9 is activated across the disease/animal model phenotypes evaluated (Figure 7D). In addition, FOXC2 and ZNF461 were identified exclusively in the hAβ-KI mice and LOAD individuals (Table S7). The three mouse models shared eight enriched MR, most of which involved in regulating cell cycle and apoptosis (Table S7). A second methodological approach to infer activation of transcription factors was also applied, and similar results were observed for the 17 master regulators candidates (Figure S8). Finally, a comparison with a previously published study that investigated MR associated with AD showed that 11 out of 17 MR identified here were also enriched in that dataset (Figure 7E).

DISCUSSION

In the past years, significant efforts of collaborative initiatives generated multiple mouse models with the aim of better recapitulating the phenotypic spectrum of sporadic LOAD. Unveiling these animal models' phenotype is a work in progress. Here, we evaluated hippocampal similarities and differences of three mouse models (APP/PS1, 5xFAD, and the novel hAβ-KI) at the transcriptional level. An exploratory cross-species comparative transcriptomics was also conducted to evaluate shared molecular core programs between these models and

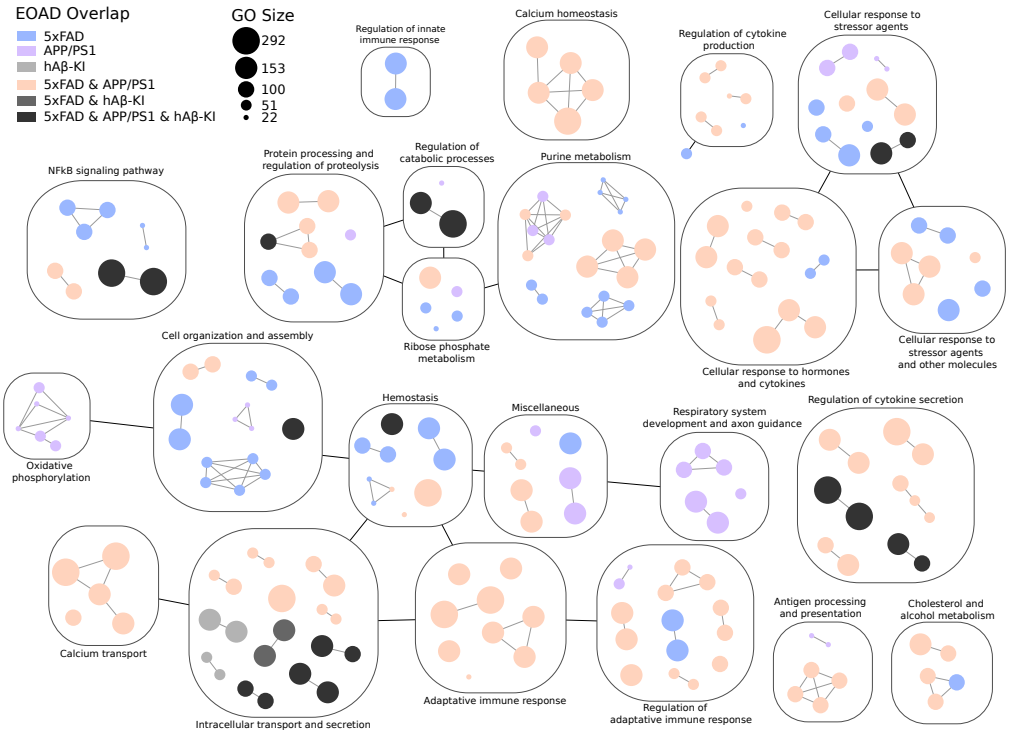

Figure 4. Nested networks of enriched GOBP intersections between EOAD and AD mouse models

Blue, purple, and orange circles represent the overlap between EOAD and protein overexpression mouse models. Intersection among EOAD and hAβ-KI is represented by the circles in shades of gray. Each box represents a cluster of GOBP terms grouped by semantic similarity and named manually according to its main biological role. Circle sizes represent the number of genes enriched in the GO term. EOAD, early-onset Alzheimer's disease; MS, multiple sclerosis; hAβ-KI, humanized amyloid-β knock-in.

EOAD/LOAD cases. All mouse models showed more similarities to LOAD than to EOAD patients. The hAβ-KI mouse model presented not only a remarkable transcriptomic similarity but also a specificity for LOAD. Surprisingly, the gene overexpressing models (i.e., APP/PS1 and 5xFAD) also better resembled LOAD than EOAD.

The specificity of the hAβ-KI model for LOAD was first observed in the exploratory DEG analysis, as hAβ-KI mice presented twice more DEGs exclusively overlapping with LOAD than with EOAD patients. Further PPI network analysis of these DEGs identified gene products that interact with each other to accomplish different biological functions. For example, we found clusters involved in ribosomal RNA processing, inflammatory response, and E3-ubiquitin ligase-related immune response, all phenomena well described in AD.[14–16] In line with this, Baglietto-Vargas et al. recently demonstrated that hAβ-KI mice presented a decreased production of the anti-inflammatory cytokines IL-2 and IL-10 compared to age-matched WT animals.[11] Importantly, a cluster of genes encoding G protein and G protein-coupled receptors (GPCRs) was also evidenced in our study. G proteins act as modulators or transducers in various transmembrane signaling systems, and GPCRs are implicated in multiple stages of AD pathogenesis.[17] Specifically, the glycogen synthase kinase 3-β (GSK3-β) is known for mediating tau phosphorylation and, consequently, being an active player in the development of tau pathology in AD.[18] Interestingly, this process seems to depend on the PI3K signaling activation,[19] a pathway significantly altered in the hAβ-KI mice. The clusters identified in our network analysis might shed light on the understanding of pathogenic mechanisms of LOAD that can be recapitulated by the novel hAβ-KI mouse model, facilitating the search for therapeutic targets.

Interestingly, only seven (C1QB, CD33, CD14, SLC11A1, S100A6, KCNK1, and SST) out of 7868 DEGs identified in our transcriptomics analysis were shared among the mouse models, EOAD, and LOAD patients. Multiple studies have already implicated these genes in AD pathophysiology. For instance, a decrease in somatostatin (SST) gene expression in AD brains has been previously reported.[20] Interestingly, SST was shown to be the most selectively enriched binder to soluble oligomeric Aβ in the human brain, influencing Aβ aggregation.[21] The consistent findings observed in our study suggest that SST role in AD pathology is conserved cross-species. Additionally, we found that C1QB, CD33, CD14, and SLC11A1 genes, all associated with immune response, were upregulated in the analyzed mouse models, as well as in EOAD and LOAD patients. Accordingly, Gjoneska et al. previously pointed a conserved immunological basis for AD by comparing the CK-p25 mouse model with hippocampal human *postmortem* tissue.[15] Our qRT-PCR analysis in APP/PS1 mice confirmed alterations in these genes. The analysis in the human brain only reached statistical significance for three of the genes – S100A6, SLC11A1, KCNK1 – but a trend was observed for SST and C1QB. This validation step indicates that our exploratory analysis provides meaningful biological information regarding AD pathology in the hippocampus.

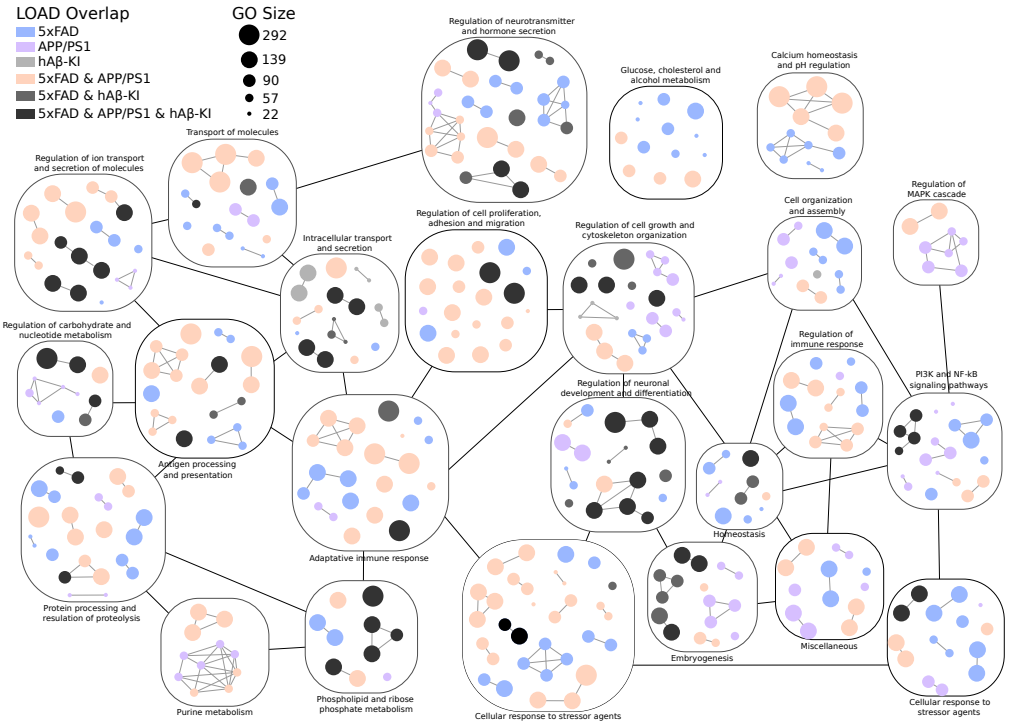

Figure 5. Nested networks of enriched GOBP intersections between LOAD and AD mouse models

Light purple, dark purple, and green circles represent all the GOBP terms overlap between LOAD and hAβ-KI. Intersection among LOAD and overexpression protein mouse models is represented by circles in shades of gray. Each box represents a cluster of GOBP terms grouped by semantic similarity and named manually according to its main biological role. Circle sizes represent the number of genes enriched in the GO term. LOAD, late-onset Alzheimer's disease; MS, multiple sclerosis; hAβ-KI, humanized amyloid-β knock-in.

Identifying transcriptomic changes at the pathway level has the potential to offer insights into the biological processes disturbed in AD. We observed that the hAβ-KI hippocampus presented an almost complete overlap of enriched hippocampal GOBP terms with LOAD, while only about one-third was shared with EOAD. This specificity for LOAD seems to be a unique and important feature of this novel KI model, as the 5xFAD and APP/PS1 mice also presented a significant overlap with EOAD. Despite that, the scanty overlap of GOBP terms among AD mouse models and MS confirmed that these models present transcriptomic features specific to AD rather than general alterations shared among other neurodegenerative diseases. In addition, this resemblance with AD appears to be a specific feature of rodent models carrying mutated human genes related to AD-associated amyloid pathology. Burns et al. observed that Tg4510 mice, which express a tau mutation found in familial frontotemporal dementia, presented the highest enrichment of genes in common with human ALS and HD rather than with AD.[22]

Early imbalance between excitatory/inhibitory (E/I) neurotransmission, with loss of neuronal network stability, is a well-attested phenomenon in AD.[23,24] The average incidence of seizure in AD patients is around 15%, which is 7-fold higher when compared to individuals without dementia.[25,26] Aβ is able to impair the long-term potentiation, promote depression of synaptic activity, alter the brain network, and affect the E/I balance by impairing the inhibitory activity of the parvalbumin-expressing and SST-expressing GABAergic interneurons.[27,28] In addition, a recent meta-analysis showed a global reduction of GABAergic system components in the human AD postmortem brain, suggesting that the GABAergic system is vulnerable to AD pathology.[30] Interestingly, modulation of GABAergic interneuron activity might improve brain rhythms and cognitive functions in AD.[27–30] Our study identified "calcium signaling" and "glutamatergic and GABAergic signaling" to be exclusively altered in the hAβ-KI mice and LOAD, pointing to this KI mouse model as an important tool to better understand calcium signaling and the E/I imbalance in AD.

Transcription factors play a key role in orchestrating phenotypic determination by regulating transcriptional targets that coordinate complex cellular processes.[13,31] We identified two transcription factors exclusively altered in the hAβ-KI model and LOAD individuals' hippocampi: ZNF461 and FOXC2. ZNF461 roles in brain function have still been poorly explored; however, this transcription factor was identified among genes that represent a polygenic risk for psychiatric disorders, and its alteration might contribute to cortical atrophy and changes in functional connectivity.[32] On the other hand, FOXC2 function in the brain is implicated in cell proliferation and invasion in glioblastoma,[33] in angiogenic processes during fetal brain development,[34] and is directly regulated by cyclin-dependent kinase 5 (Cdk5) phosphorylation to control peripheral lymphatic vase development.[35] Interestingly, it has been demonstrated that the deregulation of Cdk5 contributes to AD pathology preceding tau hyperphosphorylation and loss of synaptic proteins.[36] Several studies using organotypic hippocampal slices and primary neural cells exposed to Aβ showed increased p25 generation independently of APP overexpression,[37–39] suggesting that experimental validation of FOXC2 and Cdk5 in hAβ-KI mice is needed to understand the potential link among FOXC2, Cdk5, and AD pathology.

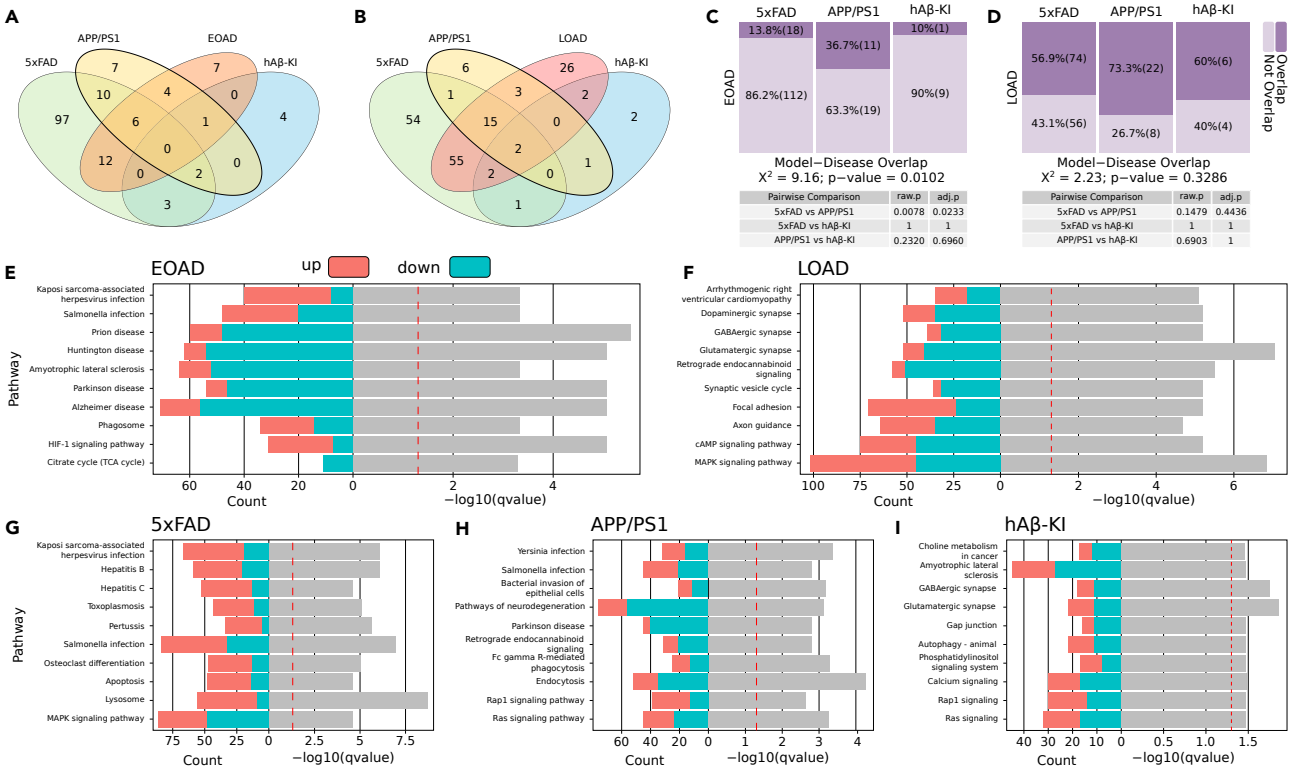

Figure 6. Functional enrichment analysis of KEGG terms in mouse models of AD and human disease

Venn diagrams showing the KEGGs overlap among EOAD (A) and LOAD (B) patients with 5xFAD, APP/PS1, and hAβ-KI mice. Mosaic plot of 5xFAD, APP/PS1, and hAβ-KI KEGGs overlap with EOAD (C) or LOAD (D). Dual-plots showing the up- (red) and down- (blue) regulated KEGGs for EOAD (E), LOAD (F), 5xFAD (G), APP/PS1 (H), and hAβ-KI (I). The size of the red and yellow boxes reflects the proportion of overlapping and non-overlapping KEGGs, respectively. Pearson's Chi−squared test with Yates' continuity correction was applied for the mosaic plot analysis. The pathways in the dual-plots are represented in the Y axis; the left and the right part of the X axis corresponds to the number of genes enriched in the KEGG terms and their q-value (gray bars), respectively. EOAD, early-onset Alzheimer's disease; LOAD, late-onset Alzheimer's disease; MS, multiple sclerosis; hAβ-KI, humanized amyloid-β knock-in.

In the MR analysis, we identified SOX9 and PARK2 as transcription factors consistently activated in the mouse models and human AD. SOX9 is a key factor in the nervous system development, especially for astrocyte and oligodendrocyte cell fate specification.[40–42] Recently, Sun et al. identified SOX9 as an astrocyte-specific nuclear marker in the adult human and mouse brains, presenting a remarkable expression in the murine hippocampus and cortex compared to the cerebellum.[43] However, there are no studies to date linking this transcription factor with AD, and our results highlight a promising new target for investigation in AD. PARK2 encodes an E3 ubiquitin ligase, and its involvement in autosomal recessive parkinsonism is well established. Although less explored, its role in AD has already been demonstrated by computational[13,44] and experimental[45–47] approaches. Specifically, mitophagy failure, promoted by repression in PARK2 ability to stimulate PS1, was reported in cellular and animal models.[45–47] On the other hand, the overexpression of PARK2 promoted diminished brain accumulation of ubiquitinylated proteins, improved its targeting to mitochondria, and potentiated autophagic vesicle synthesis.[46] Our findings thus highlight the value of hAβ-KI, 5xFAD, and APP/PS1 mouse models to better understand these particularly underexplored aspects in AD.

Decades of use of animal models in AD research underline that each of them can mimic a slightly different aspect of the disease. Therefore, one could argue that animal models of AD should be selected according to the biological aspect aimed for investigation rather than be seen as a generic model. The clusterization by semantic similarity of enriched GOBP terms performed here allowed highlighting alterations specific to 5xFAD, APP/PS1, or hAβ-KI mouse models. For example, several GOBP terms associated with oxidative phosphorylation, purine metabolism, and the MAPK pathway were altered in 5xFAD and APP/PS1 mice but not in the hAβ-KI model. On the other hand, inflammatory-related processes seem to be a feature of AD pathology present in all three mouse models. Thus, the comparison of altered biological processes among mouse models and human AD presented here sheds light on the translational power of each animal model and helps to improve our mechanistic understanding of AD pathology.

Limitations of the study

This study attempts to unveil core molecular functions in three AD animal models and compare them with AD human pathology transcriptomic profiles. To increase the sensitivity for detecting biological processes and pathways, genes with unadjusted p value <0.05 were

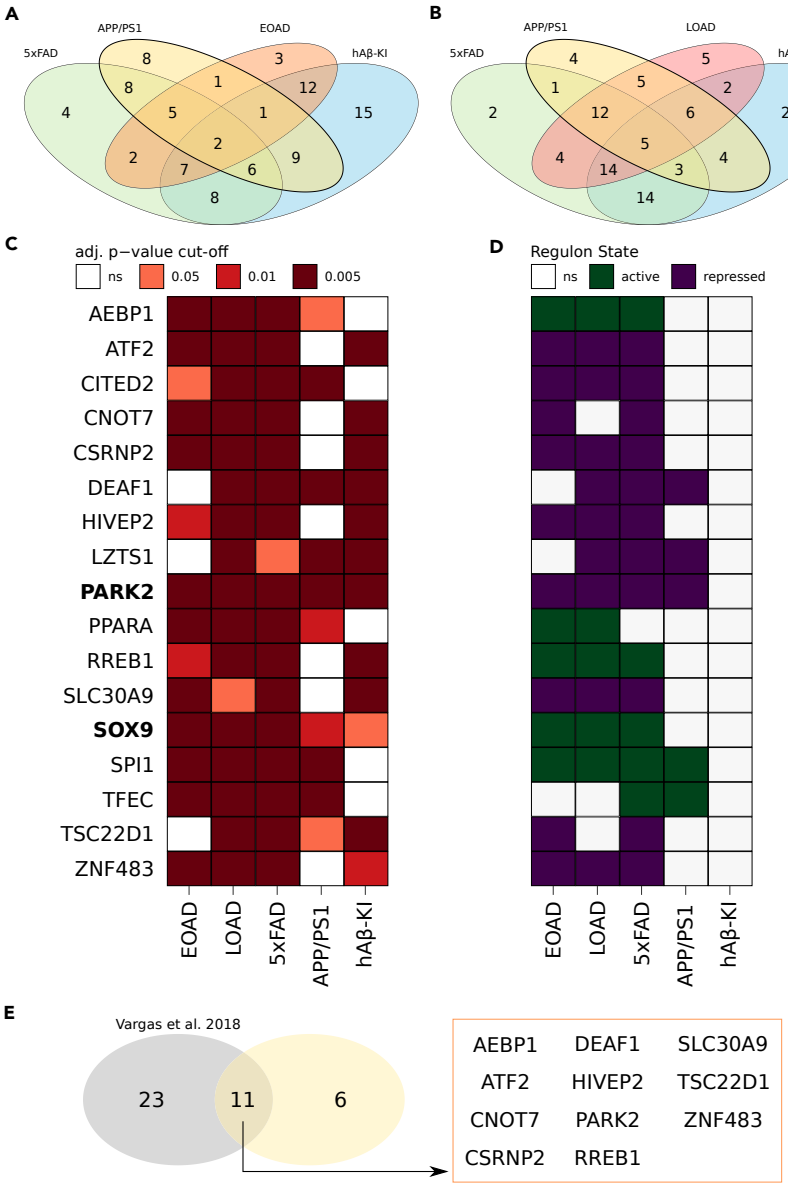

Figure 7. Master regulator analysis of mouse models of AD and human disease

Venn diagrams of EOAD (A) or LOAD (B) with 5xFAD, APP/PS1, and hAβ-KI MRs overlap. Tile-plot of regulons significantly enriched with DEGs in EOAD, LOAD, 5xFAD, APP/PS1, and hAβ-KI (only regulatory units significant in ≥4 contexts are represented). (C) Tile-plot showing the activation state of the transcription factors acting as MR in EOAD, LOAD, 5xFAD, APP/PS1, and hAβ-KI. (D) Venn diagram showing the overlap between previously MR candidates found by Vargas et al.[13] and the current study. (E) EOAD, early-onset Alzheimer's disease; LOAD, late-onset Alzheimer's disease; hAβ-KI, humanized amyloid-β knock-in; ns, non-significant.

considered as DEGs. We experimentally validated the consistently altered genes found in our study in the APP/PS1 mouse model and human brain samples. However, the functional changes inferred from DEGs in our study should be further investigated in future studies.

STAR★METHODS

Detailed methods are provided in the online version of this paper and include the following:

- KEY RESOURCES TABLE
- RESOURCE AVAILABILITY
  - Lead contact
  - Materials availability
  - Data and code availability

SUPPLEMENTAL INFORMATION

Supplemental information can be found online at https://doi.org/10.1016/j.isci.2023.108671.

ACKNOWLEDGMENTS

The results published here are partially based on data obtained from the AD Knowledge Portal (https://adknowledgeportal.synapse.org/) The IU/JAX and UCI MODEL-AD Center was established with funding from The National Institute on Aging (U54 AG054345-01 and AG054349). E.R.Z. receives financial support from Alzheimer's Association [AARGD-21- 850670], Alzheimer's Association and National Academy of Neuropsychology [ALZ-NAN-22-928381], CNPq [435642/2018-9], [312410/2018-2], [409066/2022-2], and [312306/2021-0], Serrapilheira Institute [Serra-1912-31365], Brazilian National Institute of Science and Technology in Excitotoxicity and Neuroprotection [465671/2014-4], FAPERGS/MS/CNPq/SESRS–PPSUS [30786.434.24734.23112017] and ARD/FAPERGS [54392.632.30451.05032021]. M.A.B. receives financial support from CNPq PDJ [150293/2019-4]. B.B. receives financial support from CAPES [88887.336490/2019-00] and Alzheimer's Association [AARFD-22-974627]. Fundação Carlos Chagas Filho de Amparo à Pesquisa do Estado do Rio de Janeiro (FAPERJ) (202.744/2019 and 010.002421/2019 to M.V.L.), Alzheimer's Association (AARG-D-615741 to M.V.L.), and Serrapilheira Institute (R-2012-37967) funded experiments at the Lourenco lab. R.A.S.L.-F. is supported by a FAPERJ Nota Dez predoctoral scholarship.

AUTHOR CONTRIBUTIONS

M.A.B. selected the databases and performed transcriptomics analysis. M.A.B., B.B., and G.C.-C. analyzed and interpreted the data and conceived figures and tables. B.B., G.C.-C., R.A.S.L.-F., M.V.L., M.Z., and P.K. collected experimental data. M.A.B. and B.B. wrote the manuscript. E.R.Z. conceived and supervised the project. G.C-C., T.A.P., S.F., A.C.M., R.A.S.L.-F., M.V.L., P.R.-N. and E.R.Z., edited and revised the manuscript for intellectual content.

DECLARATION OF INTERESTS

E.R.Z. is a member of the Scientific Advisory Board of Nintx, Co-founder and member of the Scientific Advisory Board of MASIMA and served in the Scientific Advisory Board of Novo Nordisk. M.A.B. is the CFO of MASIMA.

Received: October 11, 2022
Revised: July 11, 2023
Accepted: December 5, 2023
Published: December 7, 2023

REFERENCES

1. Reitz, C., Rogaeva, E., and Beecham, G.W. (2020). Late-onset vs nonmendelian early-onset Alzheimer disease: A distinction without a difference? Neurol. Genet. *6*, e512.
2. Cho, H., Choi, J.Y., Lee, S.H., Lee, J.H., Choi, Y.C., Ryu, Y.H., Lee, M.S., and Lyoo, C.H. (2017). Excessive tau accumulation in the parieto-occipital cortex characterizes early-onset Alzheimer's disease. Neurobiol. Aging *53*, 103–111.
3. McDade, E., Wang, G., Gordon, B.A., Hassenstab, J., Benzinger, T.L.S., Buckles, V., Fagan, A.M., Holtzman, D.M., Cairns, N.J., Goate, A.M., et al. (2018). Longitudinal cognitive and biomarker changes in dominantly inherited Alzheimer disease. Neurology *91*, e1295–e1306.
4. Möller, C., Vrenken, H., Jiskoot, L., Versteeg, A., Barkhof, F., Scheltens, P., and van der Flier, W.M. (2013). Different patterns of gray matter atrophy in early- and late-onset Alzheimer's disease. Neurobiol. Aging *34*, 2014–2022.
5. Rabinovici, G.D., Furst, A.J., Alkalay, A., Racine, C.A., O'Neil, J.P., Janabi, M., Baker, S.L., Agarwal, N., Bonasera, S.J., Mormino, E.C., et al. (2010). Increased metabolic vulnerability in early-onset Alzheimer's disease is not related to amyloid burden. Brain *133*, 512–528.
6. Schöll, M., Ossenkoppele, R., Strandberg, O., Palmqvist, S., Swedish BioFINDER Study, Jögi, J., Ohlsson, T., Smith, R., and Hansson, O. (2017). Distinct 18F-AV-1451 tau PET retention patterns in early- and late-onset Alzheimer's disease. Brain *140*, 2286–2294.
7. Morris, J.C., Weiner, M., Xiong, C., Beckett, L., Coble, D., Saito, N., Aisen, P.S., Allegri, R., Benzinger, T.L.S., Berman, S.B., et al. (2022). Autosomal dominant and sporadic late onset Alzheimer's disease share a common in vivo pathophysiology. Brain *145*, 3594–3607.
8. Saito, T., Matsuba, Y., Yamazaki, N., Hashimoto, S., and Saido, T.C. (2016). Calpain Activation in Alzheimer's Model Mice Is an Artifact of APP and Presenilin Overexpression. J. Neurosci. *36*, 9933–9936.
9. Götz, J., Bodea, L.G., and Goedert, M. (2018). Rodent models for Alzheimer disease. Nat. Rev. Neurosci. *19*, 583–598.
10. Saito, T., Matsuba, Y., Mihira, N., Takano, J., Nilsson, P., Itohara, S., Iwata, N., and Saido, T.C. (2014). Single App knock-in mouse models of Alzheimer's disease. Nat. Neurosci. *17*, 661–663.
11. Baglietto-Vargas, D., Forner, S., Cai, L., Martini, A.C., Trujillo-Estrada, L., Swarup, V., Nguyen, M.M.T., Do Huynh, K., Javonillo, D.I., Tran, K.M., et al. (2021). Generation of a humanized Abeta expressing mouse demonstrating aspects of Alzheimer's disease-like pathology. Nat. Commun. *12*, 2421.
12. Serneels, L., T'Syen, D., Perez-Benito, L., Theys, T., Holt, M.G., and De Strooper, B. (2020). Modeling the beta-secretase cleavage site and humanizing amyloid-beta precursor protein in rat and mouse to study Alzheimer's disease. Mol. Neurodegener. *15*, 60.
13. Vargas, D.M., De Bastiani, M.A., Zimmer, E.R., and Klamt, F. (2018). Alzheimer's disease master regulators analysis: search for potential molecular targets and drug repositioning candidates. Alzheimer's Res. Ther. *10*, 59.
14. Ding, Q., Markesbery, W.R., Chen, Q., Li, F., and Keller, J.N. (2005). Ribosome dysfunction is an early event in Alzheimer's disease. J. Neurosci. *25*, 9171–9175.
15. Gjoneska, E., Pfenning, A.R., Mathys, H., Quon, G., Kundaje, A., Tsai, L.H., and Kellis, M. (2015). Conserved epigenomic signals in mice and humans reveal immune basis of Alzheimer's disease. Nature *518*, 365–369.
16. Hegde, A.N., Smith, S.G., Duke, L.M., Pourquoi, A., and Vaz, S. (2019). Perturbations of Ubiquitin-Proteasome-Mediated Proteolysis in Aging and Alzheimer's Disease. Front. Aging Neurosci. *11*, 324.
17. Thathiah, A., and De Strooper, B. (2011). The role of G protein-coupled receptors in the pathology of Alzheimer's disease. Nat. Rev. Neurosci. *12*, 73–87.
18. Lauretti, E., Dincer, O., and Praticò, D. (2020). Glycogen synthase kinase-3 signaling in Alzheimer's disease. Biochim. Biophys. Acta. Mol. Cell Res. *1867*, 118664.
19. Ledonne, A., Nobili, A., Latagliata, E.C., Cavallucci, V., Guatteo, E., Puglisi-Allegra, S., D'Amelio, M., and Mercuri, N.B. (2015). Neuregulin 1 signalling modulates mGluR1 function in mesencephalic dopaminergic neurons. Mol. Psychiatry *20*, 959–973.
20. Gahete, M.D., Rubio, A., Durán-Prado, M., Avila, J., Luque, R.M., and Castaño, J.P. (2010). Expression of Somatostatin, cortistatin, and their receptors, as well as dopamine receptors, but not of neprilysin, are reduced in the temporal lobe of Alzheimer's disease patients. J. Alzheimers Dis. *20*, 465–475.
21. Wang, H., Muiznieks, L.D., Ghosh, P., Williams, D., Solarski, M., Fang, A., Ruiz-Riquelme, A., Pomès, R., Watts, J.C., Chakrabartty, A., et al. (2017). Somatostatin binds to the human amyloid beta peptide and favors the formation of distinct oligomers. Elife *6*, e28401.
22. Burns, T.C., Li, M.D., Mehta, S., Awad, A.J., and Morgan, A.A. (2015). Mouse models rarely mimic the transcriptome of human neurodegenerative diseases: A systematic bioinformatics-based critique of preclinical models. Eur. J. Pharmacol. *759*, 101–117.
23. Frere, S., and Slutsky, I. (2018). Alzheimer's Disease: From Firing Instability to Homeostasis Network Collapse. Neuron *97*, 32–58.
24. Palop, J.J., and Mucke, L. (2016). Network abnormalities and interneuron dysfunction in Alzheimer disease. Nat. Rev. Neurosci. *17*, 777–792.
25. Horváth, A., Szűcs, A., Barcs, G., Noebels, J.L., and Kamondi, A. (2016). Epileptic Seizures in Alzheimer Disease: A Review. Alzheimer Dis. Assoc. Disord. *30*, 186–192.
26. Imfeld, P., Bodmer, M., Schuerch, M., Jick, S.S., and Meier, C.R. (2013). Seizures in patients with Alzheimer's disease or vascular dementia: a population-based nested case-control analysis. Epilepsia *54*, 700–707.
27. Verret, L., Mann, E.O., Hang, G.B., Barth, A.M.I., Cobos, I., Ho, K., Devidze, N., Masliah, E., Kreitzer, A.C., Mody, I., et al. (2012). Inhibitory interneuron deficit links altered network activity and cognitive dysfunction in Alzheimer model. Cell *149*, 708–721.
28. Martinez-Losa, M., Tracy, T.E., Ma, K., Verret, L., Clemente-Perez, A., Khan, A.S., Cobos, I., Ho, K., Gan, L., Mucke, L., et al. (2018). Nav1.1-Overexpressing Interneuron Transplants Restore Brain Rhythms and Cognition in a Mouse Model of Alzheimer's Disease. Neuron *98*, 75–89.e5.
29. Tong, L.M., Djukic, B., Arnold, C., Gillespie, A.K., Yoon, S.Y., Wang, M.M., Zhang, O., Knoferle, J., Rubenstein, J.L.R., Alvarez-Buylla, A., and Huang, Y. (2014). Inhibitory interneuron progenitor transplantation restores normal learning and memory in ApoE4 knock-in mice without or with Abeta accumulation. J. Neurosci. *34*, 9506–9515.
30. Carello-Collar, G., Bellaver, B., Ferreira, P.C.L., Ferrari-Souza, J.P., Ramos, V.G., Therriault, J., Tissot, C., De Bastiani, M.A., Soares, C., Pascoal, T.A., et al. (2023). The GABAergic system in Alzheimer's disease: a systematic review with meta-analysis. Mol. Psychiatry *1*.
31. Carro, M.S., Lim, W.K., Alvarez, M.J., Bollo, R.J., Zhao, X., Snyder, E.Y., Sulman, E.P., Anne, S.L., Doetsch, F., Colman, H., et al. (2010). The transcriptional network for mesenchymal transformation of brain tumours. Nature *463*, 318–325.
32. Lee, A., Shen, M., and Qiu, A. (2017). Psychiatric polygenic risk associates with cortical morphology and functional organization in aging. Transl. Psychiatry *7*, 1276.
33. Li, W., Fu, X., Liu, R., Wu, C., Bai, J., Xu, Y., Zhao, Y., and Xu, Y. (2013). FOXC2 often overexpressed in glioblastoma enhances proliferation and invasion in glioblastoma cells. Oncol. Res. *21*, 111–120.
34. Siegenthaler, J.A., Choe, Y., Patterson, K.P., Hsieh, I., Li, D., Jaminet, S.C., Daneman, R., Kume, T., Huang, E.J., and Pleasure, S.J. (2013). Foxc1 is required by pericytes during fetal brain angiogenesis. Biol. Open *2*, 647–659.
35. Liebl, J., Zhang, S., Moser, M., Agalarov, Y., Demir, C.S., Hager, B., Bibb, J.A., Adams, R.H., Kiefer, F., Miura, N., et al. (2015). Cdk5 controls lymphatic vessel development and function by phosphorylation of Foxc2. Nat. Commun. *6*, 7274.
36. Kurbatskaya, K., Phillips, E.C., Croft, C.L., Dentoni, G., Hughes, M.M., Wade, M.A., Al-Sarraj, S., Troakes, C., O'Neill, M.J., Perez-Nievas, B.G., et al. (2016). Upregulation of calpain activity precedes tau phosphorylation and loss of synaptic proteins in Alzheimer's disease brain. Acta Neuropathol. Commun. *4*, 34.
37. Ma, Y., Bao, J., Zhao, X., Shen, H., Lv, J., Ma, S., Zhang, X., Li, Z., Wang, S., Wang, Q., and Ji, J. (2013). Activated cyclin-dependent kinase 5 promotes microglial phagocytosis of fibrillar beta-amyloid by up-regulating lipoprotein lipase expression. Mol. Cell. Proteomics *12*, 2833–2844.
38. Seo, J., Giusti-Rodríguez, P., Zhou, Y., Rudenko, A., Cho, S., Ota, K.T., Park, C., Patzke, H., Madabhushi, R., Pan, L., et al. (2014). Activity-dependent p25 generation regulates synaptic plasticity and Abeta-induced cognitive impairment. Cell *157*, 486–498.
39. Zheng, Y.L., Kesavapany, S., Gravell, M., Hamilton, R.S., Schubert, M., Amin, N., Albers, W., Grant, P., and Pant, H.C. (2005). A Cdk5 inhibitory peptide reduces tau hyperphosphorylation and apoptosis in neurons. EMBO J. *24*, 209–220.
40. Molofsky, A.V., Glasgow, S.M., Chaboub, L.S., Tsai, H.H., Murnen, A.T., Kelley, K.W., Fancy, S.P.J., Yuen, T.J., Madireddy, L., Baranzini, S., et al. (2013). Expression profiling of Aldh1l1-precursors in the developing spinal cord

reveals glial lineage-specific genes and direct Sox9-Nfe2l1 interactions. Glia *61*, 1518–1532.
41. Nagao, M., Ogata, T., Sawada, Y., and Gotoh, Y. (2016). Zbtb20 promotes astrocytogenesis during neocortical development. Nat. Commun. *7*, 11102.
42. Stolt, C.C., Lommes, P., Sock, E., Chaboissier, M.C., Schedl, A., and Wegner, M. (2003). The Sox9 transcription factor determines glial fate choice in the developing spinal cord. Genes Dev. *17*, 1677–1689.
43. Sun, W., Cornwell, A., Li, J., Peng, S., Osorio, M.J., Aalling, N., Wang, S., Benraiss, A., Lou, N., Goldman, S.A., and Nedergaard, M. (2017). SOX9 Is an Astrocyte-Specific Nuclear Marker in the Adult Brain Outside the Neurogenic Regions. J. Neurosci. *37*, 4493–4507.
44. Kumar, D., and Kumar, P. (2019). Abeta, Tau, and alpha-Synuclein aggregation and integrated role of PARK2 in the regulation and clearance of toxic peptides. Neuropeptides *78*, 101971.
45. Goiran, T., Duplan, E., Chami, M., Bourgeois, A., El Manaa, W., Rouland, L., Dunys, J., Lauritzen, I., You, H., Stambolic, V., et al. (2018). beta-Amyloid Precursor Protein Intracellular Domain Controls Mitochondrial Function by Modulating Phosphatase and Tensin Homolog-Induced Kinase 1 Transcription in Cells and in Alzheimer Mice Models. Biol. Psychiatry *83*, 416–427.
46. Martín-Maestro, P., Gargini, R., Perry, G., Avila, J., and García-Escudero, V. (2016). PARK2 enhancement is able to compensate mitophagy alterations found in sporadic Alzheimer's disease. Hum. Mol. Genet. *25*, 792–806.
47. Martín-Maestro, P., Gargini, R., García, E., Simón, D., Avila, J., and García-Escudero, V. (2019). Mitophagy Failure in APP and Tau Overexpression Model of Alzheimer's Disease. J. Alzheimers Dis. *70*, 525–540.
48. Unger, M.S., Li, E., Scharnagl, L., Poupardin, R., Altendorfer, B., Mrowetz, H., Hutter-Paier, B., Weiger, T.M., Heneka, M.T., Attems, J., and Aigner, L. (2020). CD8(+) T-cells infiltrate Alzheimer's disease brains and regulate neuronal- and synapse-related gene expression in APP-PS1 transgenic mice. Brain Behav. Immun. *89*, 67–86.
49. Blalock, E.M., Buechel, H.M., Popovic, J., Geddes, J.W., and Landfield, P.W. (2011). Microarray analyses of laser-captured hippocampus reveal distinct gray and white matter signatures associated with incipient Alzheimer's disease. J. Chem. Neuroanat. *42*, 118–126.
50. Miller, J.A., Woltjer, R.L., Goodenbour, J.M., Horvath, S., and Geschwind, D.H. (2013). Genes and pathways underlying regional and cell type changes in Alzheimer's disease. Genome Med. *5*, 48.
51. Hokama, M., Oka, S., Leon, J., Ninomiya, T., Honda, H., Sasaki, K., Iwaki, T., Ohara, T., Sasaki, T., LaFerla, F.M., et al. (2014). Altered expression of diabetes-related genes in Alzheimer's disease brains: the Hisayama study. Cereb. Cortex *24*, 2476–2488.
52. Berchtold, N.C., Cribbs, D.H., Coleman, P.D., Rogers, J., Head, E., Kim, R., Beach, T., Miller, C., Troncoso, J., Trojanowski, J.Q., et al. (2008). Gene expression changes in the course of normal brain aging are sexually dimorphic. Proc. Natl. Acad. Sci. USA *105*, 15605–15610.
53. Wang, M., Roussos, P., McKenzie, A., Zhou, X., Kajiwara, Y., Brennand, K.J., De Luca, G.C., Crary, J.F., Casaccia, P., Buxbaum, J.D., et al. (2016). Integrative network analysis of nineteen brain regions identifies molecular signatures and networks underlying selective regional vulnerability to Alzheimer's disease. Genome Med. *8*, 104.
54. Davis, S., and Meltzer, P.S. (2007). GEOquery: a bridge between the Gene Expression Omnibus (GEO) and BioConductor. Bioinformatics *23*, 1846–1847.
55. Leek, J.T., Johnson, W.E., Parker, H.S., Jaffe, A.E., and Storey, J.D. (2012). The sva package for removing batch effects and other unwanted variation in high-throughput experiments. Bioinformatics *28*, 882–883.
56. Voskuhl, R.R., Itoh, N., Tassoni, A., Matsukawa, M.A., Ren, E., Tse, V., Jang, E., Suen, T.T., and Itoh, Y. (2019). Gene expression in oligodendrocytes during remyelination reveals cholesterol homeostasis as a therapeutic target in multiple sclerosis. Proc. Natl. Acad. Sci. USA *116*, 10130–10139.
57. Patro, R., Duggal, G., Love, M.I., Irizarry, R.A., and Kingsford, C. (2017). Salmon provides fast and bias-aware quantification of transcript expression. Nat. Methods *14*, 417–419.
58. Soneson, C., Love, M.I., and Robinson, M.D. (2015). Differential analyses for RNA-seq: transcript-level estimates improve gene-level inferences. F1000Res. *4*, 1521.
59. Ritchie, M.E., Phipson, B., Wu, D., Hu, Y., Law, C.W., Shi, W., and Smyth, G.K. (2015). limma powers differential expression analyses for RNA-sequencing and microarray studies. Nucleic Acids Res. *43*, e47.
60. Love, M.I., Huber, W., and Anders, S. (2014). Moderated estimation of fold change and dispersion for RNA-seq data with DESeq2. Genome Biol. *15*, 550.
61. Chen, H., and Boutros, P.C. (2011). VennDiagram: a package for the generation of highly-customizable Venn and Euler diagrams in R. BMC Bioinf. *12*, 35.
62. Castro, M.A.A., Wang, X., Fletcher, M.N.C., Meyer, K.B., and Markowetz, F. (2012). RedeR: R/Bioconductor package for representing modular structures, nested networks and multiple levels of hierarchical associations. Genome Biol. *13*, R29.
63. Mora, A., and Donaldson, I.M. (2011). iRefR: an R package to manipulate the iRefIndex consolidated protein interaction database. BMC Bioinf. *12*, 455.
64. Szklarczyk, D., Gable, A.L., Lyon, D., Junge, A., Wyder, S., Huerta-Cepas, J., Simonovic, M., Doncheva, N.T., Morris, J.H., Bork, P., et al. (2019). STRING v11: protein-protein association networks with increased coverage, supporting functional discovery in genome-wide experimental datasets. Nucleic Acids Res. *47*, D607–D613.
65. Yu, G., Wang, L.G., Han, Y., and He, Q.Y. (2012). clusterProfiler: an R package for comparing biological themes among gene clusters. OMICS *16*, 284–287.
66. Yu, G., Li, F., Qin, Y., Bo, X., Wu, Y., and Wang, S. (2010). GOSemSim: an R package for measuring semantic similarity among GO terms and gene products. Bioinformatics *26*, 976–978.
67. Trabzuni, D., Ramasamy, A., Imran, S., Walker, R., Smith, C., Weale, M.E., Hardy, J., and Ryten, M.; North American Brain Expression Consortium (2013). Widespread sex differences in gene expression and splicing in the adult human brain. Nat. Commun. *4*, 2771.
68. Fletcher, M.N.C., Castro, M.A.A., Wang, X., de Santiago, I., O'Reilly, M., Chin, S.F., Rueda, O.M., Caldas, C., Ponder, B.A.J., Markowetz, F., and Meyer, K.B. (2013). Master regulators of FGFR2 signalling and breast cancer risk. Nat. Commun. *4*, 2464.
69. Margolin, A.A., Nemenman, I., Basso, K., Wiggins, C., Stolovitzky, G., Dalla Favera, R., and Califano, A. (2006). ARACNE: an algorithm for the reconstruction of gene regulatory networks in a mammalian cellular context. BMC Bioinf. *7*, S7.
70. Margolin, A.A., Wang, K., Lim, W.K., Kustagi, M., Nemenman, I., and Califano, A. (2006). Reverse engineering cellular networks. Nat. Protoc. *1*, 662–671.
71. Subramanian, A., Tamayo, P., Mootha, V.K., Mukherjee, S., Ebert, B.L., Gillette, M.A., Paulovich, A., Pomeroy, S.L., Golub, T.R., Lander, E.S., and Mesirov, J.P. (2005). Gene set enrichment analysis: a knowledge-based approach for interpreting genome-wide expression profiles. Proc. Natl. Acad. Sci. USA *102*, 15545–15550.
72. Alvarez, M.J., Shen, Y., Giorgi, F.M., Lachmann, A., Ding, B.B., Ye, B.H., and Califano, A. (2016). Functional characterization of somatic mutations in cancer using network-based inference of protein activity. Nat. Genet. *48*, 838–847.
73. Kuhn, A., Thu, D., Waldvogel, H.J., Faull, R.L.M., and Luthi-Carter, R. (2011). Population-specific expression analysis (PSEA) reveals molecular changes in diseased brain. Nat. Methods *8*, 945–947.
74. McKenzie, A.T., Wang, M., Hauberg, M.E., Fullard, J.F., Kozlenkov, A., Keenan, A., Hurd, Y.L., Dracheva, S., Casaccia, P., Roussos, P., and Zhang, B. (2018). Brain Cell Type Specific Gene Expression and Co-expression Network Architectures. Sci. Rep. *8*, 8868.

STAR★METHODS

KEY RESOURCES TABLE

REAGENT or RESOURCE	SOURCE	IDENTIFIER
Biological samples		
APPSwe/PS1ΔE9 mice on a C57BL/6J background	The Jackson Laboratories	#005864
Hippocampal tissue from LOAD, EOAD, and CU individuals	Douglas-Bell Canada Brain Bank	N/A
Critical commercial assays		
TRIzol Reagent	Invitrogen Carlbad	N/A
Applied Biosystems™ High-Capacity cDNA Reverse Transcription Kit	Applied Biosystems	N/A
Direct-zolTM RNA Microprep	Zymo Research	N/A
Deposited data		
5xFAD	AMP-AD Knowledge Portal	syn16798173
hAβ-KI	AMP-AD Knowledge Portal	syn18634479
APP/PS1	Gene Expression Omnibus (GEO)	GSE149661
APP/PS1	Gene Expression Omnibus (GEO)	GSE145907
Human AD and CU hippocampal processed microarray data	Gene Expression Omnibus (GEO)	GSE28146
Human AD and CU hippocampal processed microarray data	Gene Expression Omnibus (GEO)	GSE29378
Human AD and CU hippocampal processed microarray data	Gene Expression Omnibus (GEO)	GSE36980
Human AD and CU hippocampal processed microarray data	Gene Expression Omnibus (GEO)	GSE48350
Human AD and CU hippocampal processed microarray data	Gene Expression Omnibus (GEO)	GSE84422
MS hippocampal RNA-seq data	Gene Expression Omnibus (GEO)	GSE123496
Experimental models: Organisms/strains		
APPSwe/PS1ΔE9 mice on a C57BL/6J background	The Jackson Laboratories	#005864
Oligonucleotides		
Primers for **mouse** ACTB, C1QB, SST, CD14, CD33, SLC11A1, S100A6, KCNK1	See Table S11	N/A
Primers for **human** ACTB, C1QB, SST, CD14, CD33, SLC11A1, S100A6, KCNK1	See Table S11	N/A
Software and algorithms		
Original Codes	GitHub repository	bit.ly/46T7Xx2

RESOURCE AVAILABILITY

Lead contact

Further information and requests for resources and reagents should be directed to and will be fulfilled by the lead contact, Eduardo R. Zimmer (eduardo.zimmer@ufrgs.br).

Materials availability

Primers used for qRT-PCR and result tables in this study are provided in Tables S3 and S11.

Data and code availability

(1) RNA-seq data are publicly available as of the date of publication. Accession numbers are listed in the key resources table.
(2) Original codes are provided in GitHub [bit.ly/46T7Xx2]. Intermediate data generated are available from the corresponding author upon request.
(3) Any additional information required to reanalyze the data reported in this paper is available from the lead contact upon request.

Section 1: data

This paper analyzes existing, publicly available data. These accession numbers for the datasets are listed in the key resources table. All data reported and not included in this paper will be shared by the lead contact upon request.

Section 2: code

Original codes are provided in GitHub [bit.ly/46T7Xx2].

Section 3

Any additional information required to reanalyze the data reported in this paper is available from the lead contact upon request.

EXPERIMENTAL MODEL AND STUDY PARTICIPANT DETAILS

Mouse animal model

Male and female APPSwe/PS1ΔE9 mice on a C57BL/6J background were originally obtained from The Jackson Laboratories (#005864) and bred at our animal facility. WT littermates were used as controls. All genotypes were confirmed before use and reconfirmed after tissue extraction. Animals were housed in groups of up to five per cage with food and water *ad libitum*, under a 12 h light–dark cycle, with controlled room temperature. For qRT-PCR experiments, the whole hippocampus of 14 APP/PS1 (12-16 months-old) and 16 WT mice (12-15 months-old) were used. Institutional Permission (IRC) Information ethical committee was approved under the approval number 37248.

Human postmortem tissue

Globally sampled hippocampal tissue from LOAD (n = 8, mean ± SD age = 79.5 ± 5.6, 2F/6M), EOAD (n = 7, mean ± SD age = 51.3 ± 5.6, 6F/1M), and CU individuals (n = 9, mean ± SD age = 74.6 ± 8.9, 4F/5M) were obtained from the Douglas-Bell Canada Brain Bank with the approval of the scientific journal of the Brain Bank and the research ethics boards of the Douglas Institute (approval number: IUSMD20-02).

METHOD DETAILS

Mouse models data acquisition

RNA sequencing (RNA-seq) data from 5xFAD [4, 8, and 12 months-old, n = 23 hemizygous; 26 WT] and hAβ-KI (22 months-old, n = 7 homozygous; 8 WT) AD mouse models (Table S7) were obtained from AMP-AD Knowledge Portal (https://adknowledgeportal.synapse.org/) using *synapser* (version 0.7.64) and *synapserutils* (version 0.1.6) packages. Specifically, gene expression information was collected from https://www.synapse.org/#!Synapse:syn16798173 and https://www.synapse.org/#!Synapse:syn18634479 for 5xFAD and hAβ-KI models, respectively. APP/PS1 (8 and 12 months-old, n = 8 APP/PS1; 8 WT) mouse model RNA-seq data (Table S7) was combined from two Gene Expression Omnibus (GEO) (https://www.ncbi.nlm.nih.gov/geo/) datasets [GSE149661[48] and GSE145907] and downloaded through NCBI Sequence Read Archive using SRAToolKit (https://github.com/ncbi/sra-tools). After quality control evaluation, the following samples were removed: sample "67-2" from hAβ-KI and samples "466", "305", "456", and "497" from 5xFAD. Known phenotypic features of the three mouse models evaluated in this study are depicted in Figure S10A.

Human data acquisition

Human AD hippocampal processed microarray data of five studies were obtained from GEO repository [GSE28146,[49] GSE29378,[50] GSE36980,[51] GSE48350,[52] and GSE84422[53]], downloaded using GEOquery[54] package (v2.56.0), and combined under common gene symbol annotations. Afterward, batch correction was implemented using the sva[55] package (v3.36.0) and data was split into EOAD (age at death <65, n = 4 EOAD; 10 CU) and LOAD (age at death ≥65, n = 59 LOAD; 63 CU) for further analyses (Table S7; Figure S10). AD diagnosis, control definition, and exclusion criteria of each GSE study are depicted in Figure S10B. MS (n = 5 MS; 5 control) hippocampal RNA-seq data (Table S7) was also obtained from GEO under the identifier GSE123496[56] and downloaded through NCBI Sequence Read Archive. Sample demographics from EOAD, LOAD, and MS individuals can be found in Figure S10C.

RNA sequencing processing

Raw data for each RNA-seq dataset was downloaded and transcript alignment was performed using Salmon[57] (v1.3.0). Transcripts were mapped to genome using indexes derived from *Mus musculus* GRCm38 Ensembl build (ftp://ftp.ensembl.org/pub/release-96/fasta/mus_musculus) and *Homo sapiens* GRCH38 Ensembl build (ftp://ftp.ensembl.org/pub/release-96/fasta/homo_sapiens) for the mouse models and human data, respectively. Aligned reads were summarized using tximport[58] (v1.12.3) and genes with minimum mean of counts per million cut-off <2 were filtered out. Importantly, each mouse dataset was processed and evaluated independently. All expression data for each dataset used can be found in Table S8.

Differential expression analyses

Differential expression was computed on processed microarray data using the limma[59] package *lmFit* function to fit multiple linear models by generalized least squares. In addition, *eBayes* function was used to compute moderated t-statistics, moderated F-statistic and log-odds of differential expression by empirical Bayes moderation of the standard errors toward a common value. For RNA-seq datasets, processed expression data from each study was submitted to DESeq2[60] (v1.28.1) method using previously created tximport Summarized Experiment. Differential expression analysis (DEA) based on the Negative Binomial distribution was computed with the *DESeq* function followed by log fold change shrinkage with the *lfcShrink* function (shrinkage estimator type = "ashr"). Genes with unadjusted p value <0.05 were

considered as DEGs. For information about BH adjusted p values, see Table S1. All metadata and annotation information for the expression tables can be found in Tables S9 and S10.

Venn diagrams for DEGs were constructed using VennDiagram[61] package (v1.6.20). The proportion differences between overlapped genes between models and diseases were computed by Pearson's Chi−squared test with Yates' continuity correction for count data, followed by post-hoc pairwise Bonferroni adjustment. We compared the overlap of DEGs considering (i) the model-disease, where we obtained the number/proportion of molecular alterations observed in the models that are associated with the disease and (ii) the disease-model, where we explored how much of the total transcriptomic alteration of the disease each model captures. Together both metrics can give a measurement of fitness for modeling the pathology.

Protein-protein interaction network reconstruction

We used the Search Tool for the Retrieval of Interacting Genes/Proteins (STRING) Consortium to build PPI networks. STRING is a biological database and web resource of known and predicted PPI which contains information from numerous sources, including experimental data, computational prediction methods and public text collections. The construction of the PPI networks was implemented in R using the STRINGdb (v2.0.2), RedeR (v1.36.0), and igraph (v1.2.6) packages.[62–64] For the final networks, we retained only the edges with a combined interaction score >0.7 from all sources and highly connected nodes for the final networks.

Functional enrichment analyses

DEGs (unadjusted p value <0.05) from human or mouse model studies were submitted to GO and KEGG enrichment analyses using the clusterProfiler[65] package (v3.16.1) *enrichKEGG* and *enrichGO* functions. The GO terms were clustered by semantic similarity using the *mgoSim* function from GOSemSim[66] (v2.14.2) package (arguments measure = "Wang" and combine = NULL). The resulting similarity matrices were represented as GO networks using the RedeR (v1.36.0) package for interactive visualization and manipulation of nested networks. Clusters of GO terms obtained from GOSemSim algorithm were manually named for their biological interpretation. Venn diagrams for enriched GO/KEGG terms were constructed using VennDiagram (v1.6.20) package. Nested networks were constructed by maintaining only the intersecting GOBP terms among the mouse models and each human pathology (either EOAD or LOAD). Finally, Jaccard coefficient >0.7 was used to filter out edges with low gene intersection between terms. The proportion differences between overlapped terms between models and diseases were computed by Pearson's Chi−squared test with Yates' continuity correction for count data, followed by post-hoc pairwise Bonferroni adjustment.

Reverse engineering of transcriptional network

The transcriptional network (TN) centered on transcription factors (TF) and their predicted target genes were inferred using a large cohort of neurologically and neuropathologically normal individuals (n = 122) obtained from GEO under the identifier GSE60862.[67] Herein, the terms "regulatory unit" or "regulon" are used to describe the groups of inferred genes and their associated TFs. RTN (v2.12.1) package was used to reconstruct and analyze TNs based on the mutual information (MI) using the Algorithm for the Reconstruction of Accurate Cellular Networks (ARACNe) method.[68–70] In summary, the regulatory structure of the network is derived by mapping significant associations between known TFs and all potential targets. To create a consensus bootstrap network, the interactions below a minimum MI threshold are eliminated by a permutation step and unstable interactions are additionally removed by bootstrap. Finally, data processing inequality algorithm is applied with null tolerance to eliminate interactions that are likely to be mediated by a third TF. The reference hippocampus TN was built using the package's default number of 1000 permutations and 100 bootstraps (p value <0.001).

Master regulators inference and two-tailed gene set enrichment analysis

Master regulator analysis (MRA) was employed for the MR inference.[31] MRA computes the statistical overrepresentation of DEGs (p value <0.05) obtained from DEA in the regulatory units of the reference TN. The regulons were considered altered in the disease if they presented (1) statistical enrichment of DEGs, (2) regulon size >50, and (3) $\geq$ 80% of the queried case-control studies. Two-tailed Gene Set Enrichment Analysis (GSEA) was also performed using the RTN package (version 2.4.6, p value <0.05 and 1000 permutations). Briefly, Pearson's correlation was used to split the regulatory units into positively (A) and negatively (B) associated targets. Afterward, the phenotype association of each subgroup was tested using the GSEA[71] statistics, resulting in independent enrichment scores for each subgroup. Finally, we tested the differential enrichment (ESA – ESB) considering the following desirable criteria for clear association: (1) a maximum deviation from zero near opposite extremes and (2) a good separation of the two distributions. Thus, a high negative differential score implies that the regulon is repressed in the disorder phenotype, while a high positive one indicates that the regulon is induced.

Virtual inference of protein activity by enriched regulon analysis

The virtual inference of protein activity by enriched regulon analysis (VIPER) is another regulatory network-based approach to infer protein activity from gene expression profiles. Similar to MRA, VIPER systematically analyze the expression of the regulatory units previously identified by ARACNe algorithm. However, VIPER uses a fully probabilistic, yet efficient enrichment analysis framework based on analytic rank-based enrichment analysis. The analysis was implemented using the viper[72] (v1.22.0) package in R.

Mice

Male and female APPSwe/PS1ΔE9 mice on a C57BL/6J background were originally obtained from The Jackson Laboratories (#005864) and bred at our animal facility. WT littermates were used as controls. All genotypes were confirmed before use and reconfirmed after tissue extraction. Animals were housed in groups of up to five per cage with food and water *ad libitum*, under a 12 h light–dark cycle, with controlled room temperature. For qRT-PCR experiments, the whole hippocampus of 14 APP/PS1 (12-16 months-old) and 16 WT mice (12-15 months-old) were used. Institutional Permission (IRC) Information ethical committee was approved under the approval number 37248.

Human tissue

Globally sampled hippocampal tissue from LOAD (n = 8, mean ± SD age = 79.5 ± 5.6, 2F/6M), EOAD (n = 7, mean ± SD age = 51.3 ± 5.6, 6F/1M), and CU individuals (n = 9, mean ± SD age = 74.6 ± 8.9, 4F/5M) were obtained from the Douglas-Bell Canada Brain Bank with the approval of the scientific journal of the Brain Bank and the research ethics boards of the Douglas Institute (approval number: IUSMD20-02).

RNA extraction and qRT-PCR

Total RNA from hippocampus of LOAD, EOAD, and CU individuals as well as APP/PS1 and WT mice were isolated using TRIzol Reagent (Invitrogen Carlbad). The concentration and purity of the RNA were determined spectrophotometrically at a ratio of 260/280. Then, 1 μg of total RNA was reverse transcribed using Applied Biosystems High-Capacity cDNA Reverse Transcription Kit (Applied Biosystems, Foster City, CA), according to manufacturer's instructions. Real-time quantitative polymerase chain reaction (qRT-PCR) was performed on an Applied Biosystems 7900HT system with SYBR green master mix (Applied Biosystems). Target mRNA levels were normalized using β-actin gene (Actb) as housekeeper and cycle threshold (Ct) values were used to calculate fold changes in gene expression relatively to CU individuals or WT mice using the $2^{-\Delta\Delta Ct}$. For the human RNA extraction, Direct-zolTM RNA Microprep from Zymo Research was used. Gene expression analysis for human samples was performed at the Institute for Research in Immunology and Cancer (IRIC) Genomics Core Facility, Université de Montréal. qRT-PCR analysis in APP/PS1 and WT mice was performed independently at Universidade Federal do Rio Grande do Sul and at Universidade Federal do Rio de Janeiro. Primers used for qRT-PCR and result tables are listed in Tables S3 and S11. Standard scores (*Z* score) of APP/PS1, EOAD, and LOAD were compared for their difference from control using Wilcoxon test in R statistical environment.

Population-specific expression analysis

We used Population-Specific Expression Analysis[73] (PSEA) to deconvolute tissue heterogeneity and identify cell-specific expression changes in the context of cell population shifts. This method works by exploiting linear regression modeling of queried expression levels to cell type–specific reference measures. The brain cell marker reference dataset used for the PSEA method was obtained from the Brain Cell Type Specific Gene Expression Analysis (BRETIGEA) package.[74]

QUANTIFICATION AND STATISTICAL ANALYSIS

Differential expression analyses

Differential expression was computed on processed microarray data using the limma package62 lmFit function to fit multiple linear models by generalized least squares. In addition, eBayes function was used to compute moderated t-statistics, moderated F-statistic and log-odds of differential expression by empirical Bayes moderation of the standard errors toward a common value. For RNA-seq datasets, processed expression data from each study was submitted to DESeq2[60] (v1.28.1) method using previously created tximport Summarized Experiment. Differential expression analysis (DEA) based on the Negative Binomial distribution was computed with the DESeq function followed by log fold change shrinkage with the lfcShrink function (shrinkage estimator type = "ashr"). Genes with unadjusted p value <0.05 were considered as DEGs. The proportion differences between overlapped genes between models and diseases were computed by Pearson's Chi−squared test with Yates' continuity correction for count data, followed by post-hoc pairwise Bonferroni adjustment.

Functional enrichment analyses

DEGs (unadjusted p value <0.05) from human or mouse model studies were submitted to GO and KEGG enrichment analyses using the clusterProfiler package (v3.16.1) enrichKEGG and enrichGO functions. The GO terms were clustered by semantic similarity using the mgoSim function from GOSemSim[66] (v2.14.2) package (arguments measure = "Wang" and combine = NULL). The resulting similarity matrices were represented as GO networks using the RedeR[62] (v1.36.0) package for interactive visualization and manipulation of nested networks. Clusters of GO terms obtained from GOSemSim algorithm were manually named for their biological interpretation. Venn diagrams for enriched GO/KEGG terms were constructed using VennDiagram (v1.6.20) package. The proportion differences between overlapped terms between models and diseases were computed by Pearson's Chi−squared test with Yates' continuity correction for count data, followed by post-hoc pairwise Bonferroni adjustment.

Master regulators inference and two-tailed gene set enrichment analysis

Master regulator analysis (MRA) was employed for the MR inference.[31] MRA computes the statistical overrepresentation of DEGs (p value <0.05) obtained from DEA in the regulatory units of the reference TN. Two-tailed Gene Set Enrichment Analysis (GSEA) was also performed using the RTN package (version 2.4.6, p value <0.05 and 1000 permutations).

qRT-PCR

Standard scores (*Z* score) of APP/PS1, EOAD, and LOAD were compared for their difference from control using Wilcoxon test in R statistical environment.